Electron−Phonon Coupling and Vibronic Fine Structure of Light-Harvesting Complex II of Green Plants: Temperature Dependent Absorption and High-Resolution Fluorescence Spectroscopy

Erwin J. G. Peterman,*,† Tõnu Pullerits,‡ Rienk van Grondelle,† and Herbert van Amerongen†

Department of Physics and Astronomy and Institute for Molecular Biological Sciences, Vrije Universiteit, De Boelelaan 1081, 1081 HV Amsterdam, The Netherlands, and Department of Chemical Physics, Chemical Center, Lund University, Lund, Sweden

Received: July 31, 1996; In Final Form: March 24, 1997[⊗]

Polarized, site-selected fluorescence was measured for light-harvesting complex II (LHCII), the major Chl *a/b*/xanthophyll binding light-harvesting complex of green plants. Upon selective excitation in the range of 679−682 nm at 4 K, separate zero-phonon lines and phonon wings could be observed, as well as sharp lines in the vibronic region of the emission: vibronic zero-phonon lines. The maximum of the phonon wing was located 22 cm^{-1} to the red of the zero-phonon line. Forty-eight vibrational modes could be identified, and their Franck−Condon factors were estimated. From the vibrational frequencies it is concluded that the Chl *a* responsible for the emission at 4 K is monoligated and accepts a hydrogen bond on the 13^1-keto group. Also measured was the temperature dependence of the absorption spectrum of LHCII. Using the phonon wing obtained from the fluorescence measurements and an algorithm based on linear, harmonic Franck−Condon electron−phonon coupling and temperature independent inhomogeneous broadening, the temperature dependence of the low-energy part of the Q_y absorption spectrum could be simulated very well up to 220 K. Above this temperature, the simulated and experimental results start to deviate. From the simulations it is concluded that inhomogeneous broadening of the long-wavelength band(s) (676 nm and above) is 120 ± 15 cm^{-1} below 220 K, whereas the Huang−Rhys factor of the protein phonons is 0.6 ± 0.1 (at 4 K). We have modeled the results from absorption, fluorescence, hole-burning, triplet-minus-singlet absorption, and fluorescence anisotropy measurements by one Gaussian inhomogeneous distribution function (peaking near 676 nm) with the spectroscopic properties of the lowest energy state(s) at 4 K. There was a significant discrepancy between the results from the simulations and the experiments. A much better agreement could be obtained by assuming either two Gaussian distributions (centered around 676 and 680 nm with an intensity ratio of 11:1) or a non-Gaussian distribution around 676 nm. Although we cannot discriminate between these two descriptions, both simulations have in common that at least nine separate electronic states per trimer are present in the 676 (and 680 nm) band.

Introduction

In photosynthetic light-harvesting complexes, a complicated interplay between different pigment molecules is responsible for the details of light absorption and efficient energy transfer to the reaction centers where photochemistry takes place.[1] For a good understanding of the light-harvesting processes, a detailed insight into the factors that determine the absorption spectrum of the pigment−protein complexes involved is essential. The absorption spectrum of a single pigment ("site") in a protein at low temperature consists of two parts:[2,3] one that is only due to intramolecular (pure electronic and vibronic) transitions and another that reflects coupling of these transitions to the intermolecular vibrations of the protein environment (phonons). The former contributions give rise to Lorentzian-shaped zero-phonon lines (ZPLs), the widths of which are determined by the dephasing times of the excited states. The latter contributions give rise to broad wings, the phonon wings (PWs) to the blue of the ZPLs. Both contributions can only be observed separately at low temperature; at temperatures above about 100 K the PW totally masks the zero-phonon contribution. The ratio of the intensity of pure electronic and electron−phonon transitions depends on the strength of electron−phonon coupling expressed in the Huang−Rhys factor (*S*).[2,3]

The energy of the observed transitions not only depends on the type of pigment but also on interactions of the pigment with other pigments and the protein environment. Pigment−protein interactions can influence the electronic states of individual pigments via specific interactions like hydrogen bonding and ligation[4] or the polarizable Coulombic field it forms around the pigment.[5,6] Due to the glasslike disorder of the protein, the interactions with a pigment are inherently heterogeneous.[7,8] This heterogeneity leads to significant inhomogeneous broadening of the absorption bands of pigments bound to a protein. Also interactions between excited states of the pigments lead to shifting and splitting of corresponding energy levels and formation of so called excitonic states. These states have a delocalized character; i.e., the excitation is shared by several pigments. The extent of delocalization is largest when the energy differences between the levels of individual pigments and the dephasing are small compared to the interaction strength between the pigments. If on the other hand the interactions are relatively small, the excitations tend to be localized on the individual pigments.[1]

The temperature dependence of the absorption spectrum of a pigment−protein complex is, to a large extent, determined

* Author to whom correspondence is to be addressed. Tel: +31 20 4447941. Fax: +31 20 4447899. E-mail: erwinp@nat.vu.nl.
† Vrije Universiteit.
‡ Lund University.
⊗ Abstract published in *Advance ACS Abstracts,* January 1, 1997.

S1089-5647(96)02338-3 CCC: $14.00

by the coupling of the electronic transition to phonons and low-frequency intramolecular vibrations. Recently, several studies have appeared in which this temperature dependence was used to get insight into the strength of the electron−phonon coupling in pigment−protein complexes like hemeproteins,[9] the reaction center of *Rhodopseudomonas viridis*,[10] B820, the building block of the core light-harvesting complex of photosynthetic purple bacteria,[11] the reaction center of the photosystem two of green plants,[12] and the light-harvesting complex II (LHCII) of green plants.[13] In some of these studies, the electron−phonon coupling was described in terms of coupling to one mode, the mean phonon frequency,[9,12,13] although high-resolution techniques as spectral hole burning[7,8] and fluorescence site selection[3] show that a broad distribution of phonon modes is involved. In the study of the B820 complex, the electron−phonon coupling was described using the PW obtained from a low-temperature emission spectrum excited with a narrow-band laser in the red edge of the absorption spectrum.[11] This fluorescence site selection is a technique useful to obtain high-resolution information not only on electron−phonon coupling but also on vibronic coupling.[3] For instance, for several dye molecules in organic glasses, sharp vibronic zero-phonon lines (vZPLs) have been observed.[3] The information on intramolecular vibrations obtained in this way is similar (but not identical, other selection rules apply) to that obtained from Raman or infrared spectroscopy.[14] So far, vZPLs in the fluorescence of (bacterio)chlorins have only been observed for the pigments in organic solvents,[15,16] not in an intact protein environment.

In this contribution we report the observation of zero-phonon vibronic lines in the 4 K site-selective emission spectra of trimeric LHCII, the main light-harvesting antenna in green plants. About eight chlorophyll *a* (Chl *a*), six chlorophyll *b*, and several (three to four) xanthophyll molecules are thought to bind to each monomer.[17] The three-dimensional structure of trimeric LHCII as resolved with electron microscopy and electron diffraction of two-dimensional crystals[18] shows that the complex is a densely packed array of Chl molecules, about 10 Å (center to center) apart, which are imbedded in the protein matrix that contains three trans-membrane helices. In the center of the complex two xanthophyll molecules are present.

It has been shown with polarized light spectroscopy[19,20] that some degree of excitonic coupling exists between the Chl molecules. Recently, several studies have addressed the lowest energy state of LHCII,[21−24] the state responsible for emission at 4 K. The emission at 4 K peaks at 681 nm, with a width of 5.5 nm (full width at half-maximum (fwhm)).[23−25] However, no bands located to the red of the absorption maximum at 676 nm could be observed in the low-temperature circular dichroism (CD) and linear dichroism (LD) spectra[19,24] or Stark spectra,[26] and the presence of an additional band toward the red of the one at 676 nm was considered to be unlikely.[19] According to this interpretation, the fluorescence at low temperature arises from the pigment with the lowest energy in this distribution. Later, hole-burning data by Reddy and co-workers[21] showed a sharp hole near 680 nm, representing a weak lowest energy state. The width of the corresponding inhomogeneous distribution function (IDF) was ∼120 cm^{-1} (5.5 nm). The coupling of this electronic transition to protein phonons with a mean frequency of 20 cm^{-1} was characterized by a Huang−Rhys factor of 0.4−0.5**.** This weak coupling strength implies that 30−40% of the single-site absorption is due to the PW. It was demonstrated that the 680 nm band, which has an intensity of about one Chl *a* per trimer, is sometimes accompanied by satellite holes (at 674 and 678 nm). The possibility was put forward that the 680 nm band is excitonically related to the 678 and 674 nm bands. The ZPL distribution was largely uncorrelated to those of the higher energy states in the Q_y region. In a recent study of triplet states in LHCII, we have also observed a band at 680 nm (width ∼6 nm) in the Chl *a* and xanthophyll triplet-minus-singlet absorption (T−S) spectra measured at 4 K.[27] Zucchelli and co-workers[13] measured the absorption spectrum of LHCII at different temperatures between 71 K and room temperature. At all temperatures the Q_y absorption spectrum was fitted with a set of asymmetric Gaussians. The authors modeled the temperature dependence of the widths of the individual bands, assuming that the inhomogeneous broadening is constant (see above). They arrived at values for *S* of 0.45−0.75 and inhomogeneous widths of ∼120 cm^{-1} for two bands at 672 and 678 nm, respectively. These values imply that the inhomogeneous broadening does not exceed the homogeneous widths of the subbands at room temperature, in accordance with recent results by Lokstein and co-workers.[28] Also a weak band around 684 nm was fitted, which gained intensity from 4% at 71 K to 16% at 296 K. Savikhin and co-workers[22] measured the temperature dependence of the pump−probe anisotropy decay in LHCII. They observed an increase of the anisotropy decay time at the low-energy side of the absorption spectrum (680−682 nm) with a factor of 5−6 going from room temperature to 13 K. This data could be simulated with a model accounting for temperature dependence of Förster energy transfer rates caused by the temperature dependence of the spectral overlap of donor and acceptor. The data could be explained reasonably well by invoking two distinct bands (near 680 and 675 nm) with inhomogeneous widths of 100−150 cm^{-1}, in accordance with other studies.[19,21,24]

Earlier, we have studied LHCII using polarized site-selective fluorescence spectroscopy.[23] In these measurements the spectral resolution was too low to observe separate ZPLs and PWs. In the present article we will show new experiments with higher wavelength resolution and sensitivity, at temperatures ranging from 4 K to room temperature, and use the results to simulate the temperature dependence of the red part of the absorption spectrum.

Materials and Methods

Sample Preparation. Trimeric LHCII was prepared and purified using the method described earlier[27] based on anion-exchange chromatography and using the detergent *n*-dodecyl-*β*,D-maltoside (DM) for solubilization of the complexes. For the low-temperature measurements LHCII was diluted in a buffer containing 20 mM Hepes (pH 7.5), 0.06% (w/v) DM, and 70% (v/v) glycerol. The optical density of the samples was typically 0.2 cm^{-1} at 675 nm and for the anisotropy measurements 0.05 cm^{-1}. The temperature of the sample was regulated using a helium bath cryostat (Utreks) for the fluorescence measurements or a helium flow cryostat (Oxford Instruments) for the absorption measurements.

Spectroscopy. Absorption spectra were recorded on a Cary 219 spectrophotometer using an optical bandwidth of 0.5 nm. Fluorescence emission spectra were measured with a CCD camera (Chromex Chromcam 1) via a $^1/_2$ m spectrograph (Chromex 500IS). An optical bandwidth of 0.5 or 0.25 nm was used. In the latter case, a point was recorded every 0.035 nm. The wavelength calibration of the detection system was checked with an argon calibration lamp. Emission spectra were corrected for the wavelength sensitivity of the detection system. A dye laser (Coherent CR599, dye DCM) pumped by an argon-ion laser (Coherent Inova 310) was used as a narrow-banded excitation source in the wavelength region from 640 to 710 nm. The optical bandwidth of excitation was ∼0.1 nm. At temper-

atures of 77 K and below, the laser power was kept below 0.2 mW/cm^2 to prevent spectral hole burning. The typical illumination time was 1 min per excitation wavelength. Even using these low-illumination doses, we observed a small decrease (maximal ~10%) in the fluorescence intensity of consecutively measured spectra, indicating the extreme care that should be taken when resonantly exciting Chl *a*-containing systems at liquid helium temperatures using laser light. At each temperature emission spectra were measured for 15−25 different excitation wavelengths between 650 and 710 nm. For the 0.5 nm detection bandwidth scans polarizers were used in the excitation and emission branches of the setup to be able to calculate the anisotropy ($r(\lambda)$) of the emission according to

$$r(\lambda) \equiv \frac{F_{||}(\lambda) - F_{\perp}(\lambda)}{F_{||}(\lambda) + 2F_{\perp}(\lambda)} \quad (1)$$

in which $F_{||}(\lambda)$ and $F_{\perp}(\lambda)$ are the (corrected) emission spectra with polarization parallel and perpendicular to the polarization of the excitation. The anisotropy was read from the curves between 700 and 710 nm. Isotropic emission spectra ($F_{iso}(\lambda)$) were calculated as

$$F_{iso}(\lambda) \equiv F_{||}(\lambda) + 2F_{\perp}(\lambda) \quad (2)$$

Simulation of the Temperature Dependence of Absorption and Fluorescence. The temperature dependence of the main (676 nm) band in the absorption spectrum of LHCII was simulated using the algorithm applied before on B820.[11] The simulation is based on the assumption that the temperature effects in the absorption spectrum are caused by linear harmonic Franck−Condon interaction of the electronic transitions with protein phonons and low-frequency intramolecular vibrations of the chromophore.[2,3] The calculation algorithm has been described extensively.[11] In short, it is based on the numerical extraction of the one-phonon profile (φ) from the low temperature (4 K) PW (Φ) of a selectively excited (in the red of the absorption band) emission spectrum using eq 3

$$\varphi(\omega) = \frac{\Phi(\Omega + \omega)}{\alpha} - \frac{1}{\alpha\omega}\int_0^{\omega} \Phi(\Omega + \omega - \omega')\omega'\varphi(\omega')\, d\omega' \quad (3)$$

in which Ω is the frequency of the zero-phonon transition, ω is the frequency, and α is the Debye−Waller factor (e^{-S}). This one-phonon profile, which also consists of low-frequency intramolecular vibronic transitions, is used to simulate the lowest energy band of the absorption spectrum at different temperatures using

$$A(\omega,T) = \left(\sum_{i=0}^{\infty} \frac{S(T)^i\, e^{-S(T)}}{i!} l_i(\Omega - \omega)\right) \otimes \mathrm{IDF}(\omega) \quad (4)$$

$A(\omega,t)$ is the intensity of the absorption spectrum at energy ω and temperature T, i runs over the Franck−Condon progression of phonons, $S(T)$ is the effective Huang−Rhys factor at temperature T, l_i is the line shape of the i-phonon transition (a Lorentzian for the ZPL, the convolution of the one-phonon profile with l_{i-1} for the i-phonon transition), $\otimes$ is the convolution operator, and IDF(ω) is the inhomogeneous distribution function (a Gaussian). It should be noted that in this approach the IDF is temperature independent; the effective Huang−Rhys factor fully accounts for the temperature dependence

$$S(T) = S\int_0^{\infty} \varphi(\omega) \coth\left(\frac{h\omega}{2kT}\right) d\omega \quad (5)$$

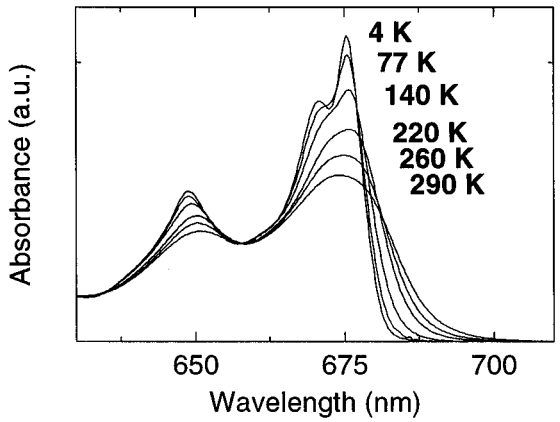

Figure 1. Absorption spectra of LHCII at temperatures between 4 and 300 K. The spectral bandwidth was 0.5 nm.

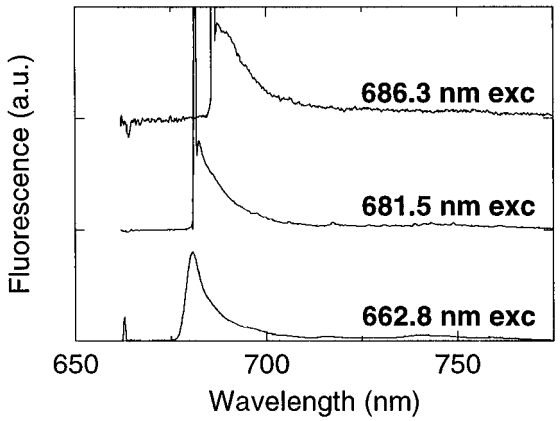

Figure 2. Isotropic emission spectra of LHCII at 4 K, at different excitation wavelengths. The spectral bandwidth of detection was 0.5 nm.

S is the Huang−Rhys factor at 0 K, and $\varphi(\omega)$ is the one-phonon profile (eq 3). The temperature dependence of the calculated bands is compared to those of the measured spectra to obtain values for S and the width of the IDF. These values can be used to simulate the absorption and emission spectra of the lowest energy band at each temperature. The comparison between experimental and simulated spectra is made on basis of the second moment of absorption (M_2, eq 6), a measure of the width of the absorption band.

$$M_0 = \int A(\omega)\, d\omega$$

$$M_1 = \frac{\int \omega A(\omega)\, d\omega}{M_0}$$

$$M_2 = \frac{\int \omega^2 A(\omega)\, d\omega}{M_0} - M_1^2 \quad (6)$$

Results

Absorption Spectra. In Figure 1 the absorption spectrum of LHCII at different temperatures is shown. The spectra are similar to those reported in earlier studies.[13,19,21,22,27] Clear is the band broadening and the apparent red shift of the whole spectrum upon increasing the temperature.

Isotropic Energy Selective Emission Spectra at Different Temperatures. In Figure 2 a few examples of the isotropic, energy selective emission spectra of LHCII at 4 K are shown. Upon excitation below ~678 nm, the shape and position of the

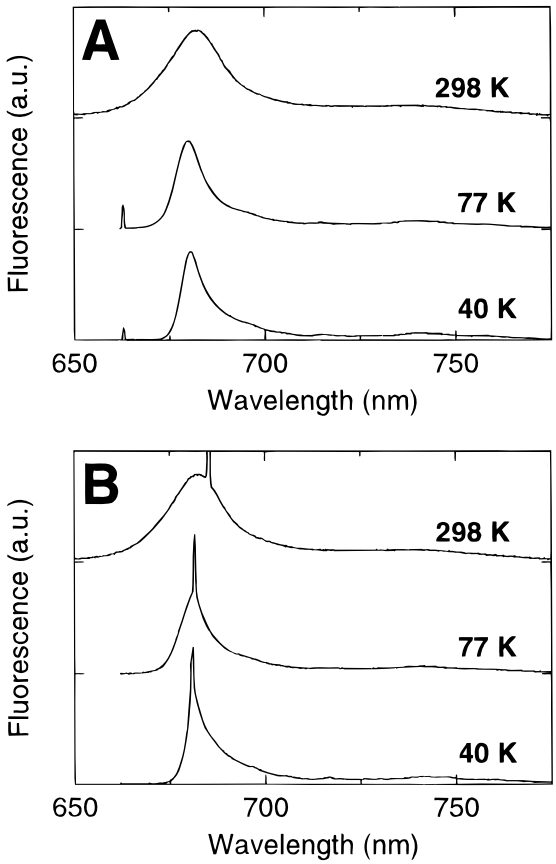

Figure 3. Nonselective (A) (excited at 663.0, 663.0, and 643.8 nm respectively) and "selective" (B) (excited at 680.9, 681.6, and 685.3 nm respectively) isotropic emission spectra of LHCII at 40, 77, and 298 K. The spectral bandwidth of detection was 0.5 nm.

emission spectra are independent of the excitation wavelength; the emission peaks at 680.7 nm and has a width of 5.7 nm (fwhm). Upon excitation more to the red (above ~680 nm), clear separate ZPLs (at the excitation wavelength, partly masked by scattering from the excitation laser) and PWs can be observed, in contrast to our earlier measurements,[23] where no separate PW could be observed. This is partly due to the higher resolution of the current experiments. However, also the lower excitation density and illumination time used probably contribute; when we applied higher intensities and longer illumination (not shown), we observed hole burning and disappearance of the fine structure. In the spectra excited between about 679 and 682 nm, sharp vibronic lines could be observed (see Figure 2 and Figure 4). To our knowledge, this is the first example of vibronic fluorescence line narrowing in an intact photosynthetic pigment−protein complex. We have measured spectra at higher resolution in this region, which will be shown and discussed below. Upon excitation below ~680 nm, the maximum of the emission is independent of the excitation wavelength. Above about 680 nm the PW, then observed separately from the ZPL, shifts linearly with the excitation wavelength. The constant separation between PW and ZPL is 1.0 nm (22 cm^{-1}). This is close to the separation of 20 cm^{-1} observed in hole burning.[21] Upon excitation above 680.5 nm, the shape of the phonon wing remains constant, suggesting that maximum selectivity has been reached.

Energy-selective fluorescence was also measured at higher temperatures. In Figure 3 emission spectra measured at some characteristic temperatures are shown.The maxima of the nonselectively excited (below 678 nm) spectra (Figure 3A) shift upon increasing the temperature from 4 to 180 K to the blue (from 680.7 to 679.0 nm). Upon further increasing the

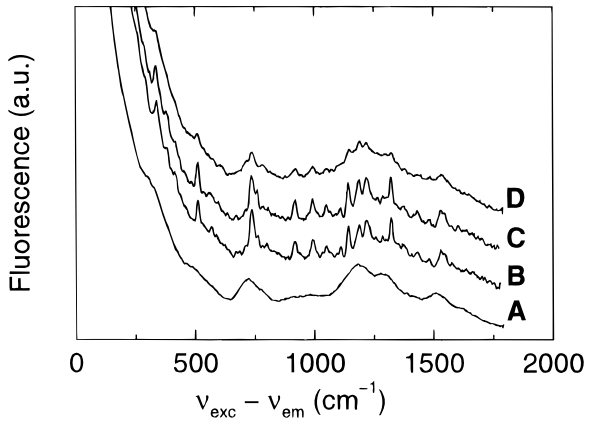

Figure 4. Vibronic region of the isotropic emission of LHCII, bandwidth of detection 0.5 nm. (A) 4 K, (aselective) excitation at 662.8 nm; (B) 4 K, (selective) excitation at 681.5 nm; (C) 15 K, excitation at 681.6 nm; (D) 40 K, excitation at 680.9 nm. Spectrum A is shifted arbitrarily to be compared best with the other spectra. For a good comparison the spectra were given equidistant offsets.

temperature, the emission shifts to the red (to 682.2 nm at room temperature). This rather peculiar temperature dependence has been observed before.[19,24] The width of the emission spectrum increases gradually from 5.7 nm at 4 K to 18.4 nm at 298 K. Some selectively excited spectra are shown in Figure 3B. The spectra measured at 15 K (not shown) are very similar to those at 4K: the ZPL can be observed separately from the phonon wing, and the vibronic fine structure is as pronounced (see below). At 40 K the phonon wing and ZPL have merged together. However, although less pronounced, the vibrational fine structure as observed at 4 and 15 K is still present. The sharp vZPLs are significantly broadened at 40 K, to about 1 nm fwhm, indicating the increase of the width of the red-most transitions at higher temperature. The vibronic fine structure is totally lost in the spectra measured at 77 K and higher. At 150 K and above, the emission spectra do not change (in shape or position) anymore upon varying the excitation wavelength. At room temperature, the spectrum excited at 710 nm (not shown) looks exactly the same as the one excited at 670 nm, although the intensity is far less.

Vibronic Fine Structure. As shown above we have observed sharp vZPLs in the emission of LHCII at low temperatures (40 K and below). In Figure 4 we show the vibronic region of the emission spectra for nonselective excitation at 4 K and selective excitation (~681 nm) at 4, 15, and 40 K. Clearly visible is the increase of resolution of the vibronic transitions upon selective excitation, which gradually disappears upon increasing the temperature. This is caused by loss of selectivity due to (uphill) energy transfer, ingrowth of anti-Stokes phonon contributions, and broadening of the homogeneous spectrum. The width of the sharp vibronic features at 4 and 15 K (in Figure 4) is limited by the resolution of the detection system. To obtain more detailed insight into the vibronic lines, we have measured the emission spectra of LHCII upon excitation at 10 different wavelengths between 679 and 682 nm at higher resolution (0.25 nm = 5.5 cm^{-1}), at both 4 and 15 K. This resolution, combined with detection of 1 point per 0.035 nm, makes a good estimation of shape and area of the vibronic bands possible. One example of such a spectrum is shown in Figure 5. Forty-eight vibronic lines could be identified in all spectra. In Table 1 all observed transitions are listed. Between 678 to 680.5 nm, the intensity of the vibronic lines compared to the background increases upon exciting more to the red. For excitation wavelengths above 680.5 nm, the

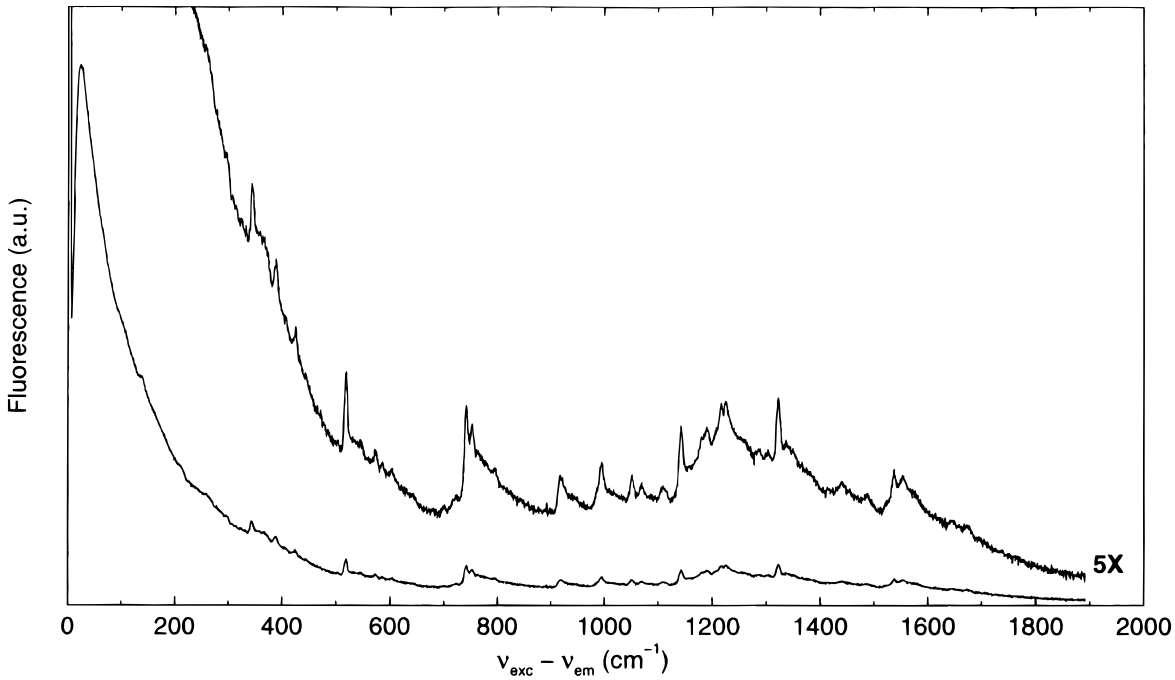

Figure 5. Emission spectrum of LHCII at 4 K upon excitation at 680.7 nm. The spectral bandwidth is 0.25 nm; no polarizer was used in the detection branch.

relative intensity of the vZPLs remains constant, indicating that above 680.5 nm maximum selectivity has been reached.

Also included in Table 1 are the Franck−Condon factors of the vibronic transitions. These have been determined by calculating the ratios of the areas of the vZPLs to that of the pure electronic ZPL (coinciding with the excitation). As these ratios are very small, they are a good approximation of the Franck−Condon factors. The area of the pure electronic transition was estimated using the PW and the Huang−Rhys factor as obtained in the next section ($S = 0.6$). The experimental pure electronic ZPL, which is contaminated with scattering from the excitation laser, was not used for the determination of the Franck−Condon factors, so interference with scattering light does not play a role. On the other hand, the area of the pure electronic ZPL depends on the Huang−Rhys factor used. Even if we use for S a value of 0.35 (1.0), instead of 0.6, we underestimate (overestimate) the ZPL area by a factor of 2 (and consequently overestimate (underestimate) the Franck−Condon factors accordingly). We think that these two extreme values for S are out of the error margins of the value of S (see below). The obtained Franck−Condon factors are significantly smaller than those reported by Gillie and co-workers[29] (see below).

Excitation Wavelength of the Anisotropy of Emission. In Figure 6 the excitation wavelength dependence of the fluorescence anisotropy at 4 K is shown. Upon increasing excitation wavelength, the anisotropy rises gradually to a value of ∼0.05 at about 676 nm. Up to this wavelength the fluorescence anisotropy is similar to the reduced linear dichroic (LD) spectrum.[19,29] Above about 680 nm part of the excitations is trapped without energy transfer and the anisotropy rises steeply to a value of 0.36 at 685 nm. This is close to the theoretical maximum of 0.4, which is reached when the fluorescence is emitted by the absorbing state; i.e., no energy transfer takes place. In previous polarized fluorescence measurements on LHCII at 4 K, we observed a maximal anisotropy of 0.24.[23] This low value might be caused by hole burning due to the ∼100 times higher excitation densities used for those measurements. The results observed now are in excellent agreement with the values of the residual anisotropy observed in pump−probe anisotropy decays of LHCII at 13 K.[22]

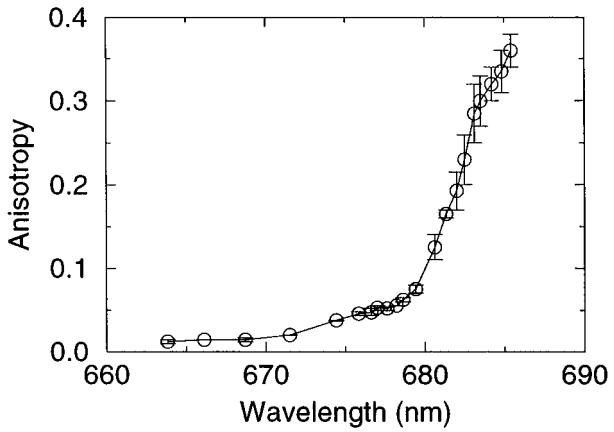

Figure 6. Anisotropy of emission of LHCII versus excitation wavelength at 4 K. Each data point corresponds to a sequence $F_{\parallel}$, $F_{\perp}$, $F_{\perp}$, $F_{\parallel}$; the circle corresponds to the average of the anisotropy as calculated from the first two spectra and the last two. The vertical lines correspond to the two extreme values. Due to hole burning the second value was always lower than the first value; the values should be considered as upper and lower limits for the true anisotropy.

Simulations and Discussion

Simulation of the Temperature Dependence of Electron−Phonon Coupling. To simulate the temperature dependence of the electron-phonon coupling in absorption of LHCII, we applied the same procedure as used before for B820.[11] We extracted numerically the PW and the one-phonon profile (after a starting value for S was chosen) from a 4 K site-selective emission spectrum excited at 681.5 nm using eq 3. From the comparison of simulated (eqs 4 and 5) and experimental temperature dependence of the absorption bands, S, and the width of the IDF can be determined in an iterative way.[11] We compared the simulated spectra to the red wing of the 676 nm absorption band of LHCII. For this simulation we assumed that this band is inhomogeneously broadened and that the IDF has a Gaussian shape. To not overestimate the absorption to the

TABLE 1: Comparison between the Vibrational Frequencies As Obtained for the Emission of LHCII at 4 K and the Estimated Franck−Condon Factors (See Text) and Literature Values for the Excited State Vibrations of Chl *a* in PS1 As Obtained from Hole Burning[29] and of the Excited and Ground-State Vibrations of Chl *a* in Ether As Obtained from Fluorescence[15]

S_0 (this study)		S_1 [29]		S_1 [15]		S_0 [15]
ω (cm^{-1}) (±2)	S (±50%)	ω (cm^{-1})	S	ω (cm^{-1})	rel. int.	ω (cm^{-1})
97 (broad)	0.000 64					
138	0.000 59					
213	0.000 32					
260	0.000 10	262	0.012	263	3	260
		283	0.004			
298	0.000 16					
342	0.001 0			348	4	350
388	0.000 76	390	0.015	390	2	390
425	0.000 44	425	0.007			
		469	0.019	465	2	470
		501	0.007			
518	0.001 3	521	0.017	515	1	520
546	0.000 089	541	0.009			
573	0.000 28	574	0.025	570	2	570
585	0.000 10	588	0.005	583	1	
604	0.000 064	607	0.012	600	1	
				635	1	
				670	1	
700	0.000 065			688	1	
722	0.000 13	714	0.010			
742	0.001 9	746	0.044	740	4	745
752	0.001 3			748	3	755
		771	0.007	765	1	
795	0.000 16	791	0.014	785	1	
		805	0.012			
		819	0.005			
		855	0.009			
		864	0.007			
		874	0.007	880	1	
		896	0.013	890	1	
				910	1	
916	0.000 74	932	0.025	925	2	915
986	0.000 34	994	0.028	984	5	987
995	0.000 80	1009	0.005	1005	1	
1052	0.000 40			1030	1	
1069	0.000 21	1075	0.012	1075	2	
1110	0.001 5	1114	0.009	1110	2	
1143	0.000 37			1135	2	1145
1181	0.000 58	1178	0.018	1168	2	1185
1190	0.000 22			1195	1	
1208	0.000 61	1203	0.012			
1216	0.000 58					
1235	0.000 23			1243	sh.	
1252	0.000 21			1250	5	
1260	0.000 21	1259	0.041			
1286	0.000 15	1285	0.011	1275	1	
1304	0.000 19					
1322	0.000 11			1325	1	1325
1338	0.000 13	1340	0.011			
1354	0.000 19	1364	0.032	1345	3	
1382	0.000 22	1390	0.018			1385
		1411	0.005	1415	1	
1439	0.000 22	1433	0.009			1430
		1455	0.005			
1487	0.000 26	1465	0.006			1485
		1504	0.010	1510	3	
1524	0.000 21	1524	0.032			1525
1537	0.000 72			1530	2	
1553	0.000 51					1545
1573	0.000 15					
1580	0.000 15					
1612	0.000 15					
1645	0.000 12					
1673	0.000 032					

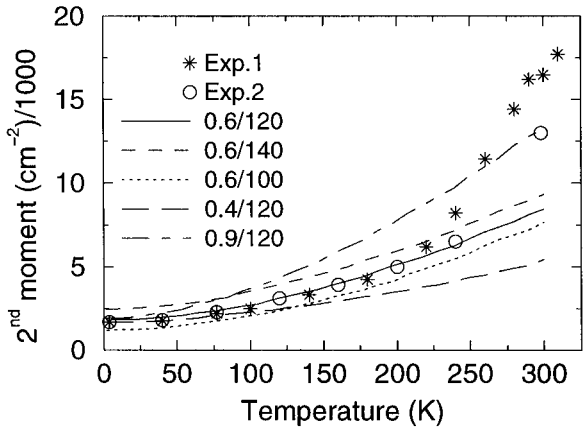

Figure 7. Comparison between the experimental (two independent data sets) and simulated temperature dependence of the second moment of the 676 nm absorption band of LHCII (see text). The values for *S* and the width of the inhomogeneous distribution were as indicated.

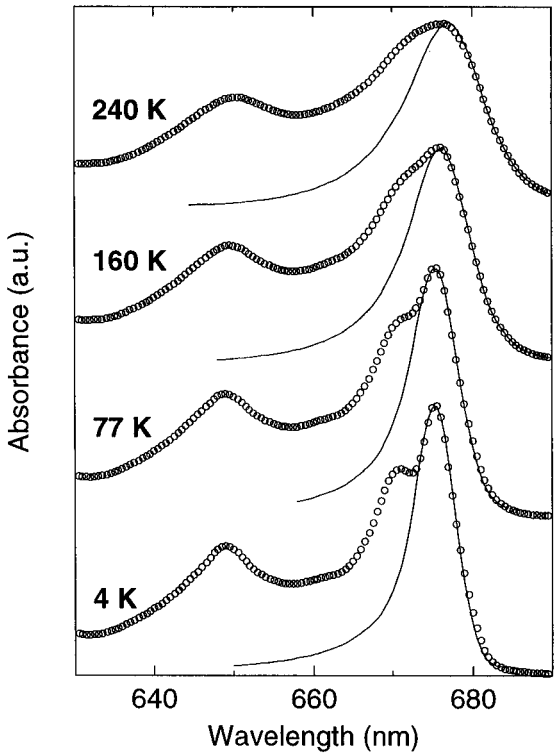

Figure 8. Comparison between experimental absorption spectrum of LHCII (circles) and the simulated 676 nm band (straight line) at 4, 77, 160, and 240 K.

red of this band (680 nm and further), we have calculated the second moment of the band starting from the maximum up to one-third of the maximum. In Figure 7 the comparison between experimental and calculated temperature dependences of the second moment of the absorption is shown. Up to 220 K the experimental data can be described very well with a value of 0.6 ± 0.1 for *S* and a fwhm of the IDF (at 676 nm) of 120 ± 15 cm^{-1}. In order to demonstrate the sensitivity of our approach, we have also shown in Figure 7 how the simulations and experimental results start to deviate when other values for *S* and the fwhm of the IDF are used. In Figure 8 a comparison is shown of experimental absorption spectra and simulations of the 676 nm band at several temperatures. Except for the very red edge of the band (above 680 nm), the similarity between fit and simulation is satisfactory. The shift of the peak position with temperature, which might be due to quadratic and/or anharmonic electron−phonon coupling,[6,9] was not accounted

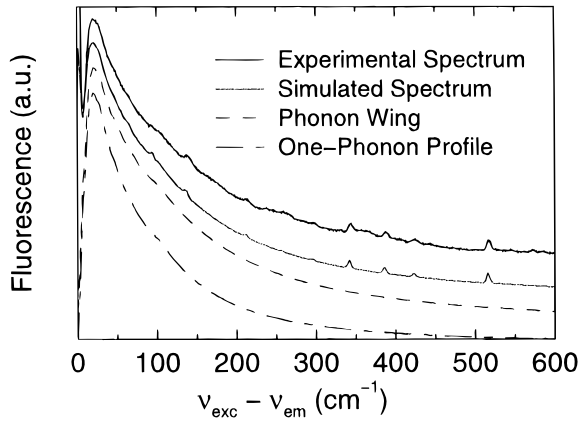

Figure 9. Experimental and simulated (see text) site-selective fluorescence spectrum of LHCII at 4 K (excitation at 681.5 nm), the phonon wing extracted, the site-selective fluorescence spectrum, and the one-phonon profile extracted from the phonon wing (see text). For a good comparison the spectra were given equidistant offsets.

for in our simulations. The maxima of the simulated bands in Figure 8 are shifted to coincide with the experimental spectra. In Figure 9 the PW, the one-phonon profile (assuming $S = 0.6$), and a simulated and an experimental site-selective emission spectrum are shown. The simulated site-selective emission spectrum was constructed using the Franck−Condon factors listed in Table 1 and a width of 5 cm^{-1} for the (v)ZPLs (the resolution of detection).

The value for *S* as estimated from our simulations of the temperature dependence of the absorption spectrum (0.6) is comparable, though slightly larger than the one obtained from hole burning[21] ($S = 0.4-0.5$). The temperature dependence of the LHCII absorption spectrum was also modeled by Zucchelli and co-workers.[13] Their method, parallel fitting of the absorption spectra at different temperatures with Gaussian bands, did not allow an estimation of the value of *S*. However, the obtained value of the inhomogeneous width (117 cm^{-1} for a fitted band at 678 nm) agrees quite well with the value obtained in the present study.

Above 220 K the simulations do not describe the experimental data anymore. One obvious reason for this is that above 220 K the 672 and 676 nm absorption bands start to merge, which makes the determination of the second moment of only the 676 nm band difficult. However, the deviation from the simulation is rather large and as noted above also the peak position of the nonselective emission starts to shift to the red above about 220 K. So it is very likely that above 220 K the properties of the lowest energy part of the LHCII absorption spectrum change. Different effects might start to play a role: changes in the IDF (increase of the width) and/or changes in the electron−phonon coupling (nonlinearity). Both might be caused by the transition from a solid-like to a more flexible, fluid-like protein environment at higher temperatures. Interesting to note is that a similar deviation for the temperature dependence of the absorption spectrum as modeled using a comparable model has been found for several heme proteins[9] and the reaction center of *Rps. viridis*.[10] Simulations of excited-state energy equilibration in LH-1 of *Rhodobacter sphaeroides* suggest a doubling of the inhomogeneous width at room temperature (400 cm^{-1}) as compared to 4 K (200 cm^{-1}).[31]

In the Gaussian fits of Zucchelli and co-workers,[13] a 684 nm band was needed for proper fitting, which has a pronounced temperature dependence. The possibility was put forward that this band is a vibronic transition (1,0 ← 0,1), to the red of the main (1,0 ← 0,0) transition. Using Bose−Einstein statistics, it was calculated that the corresponding vibrational mode has a frequency of about 120 cm^{-1} and a value of $S = 0.4$ is needed. However, in our selectively excited emission spectra, there is no support for existence of such a relatively strongly coupled mode. We found that the coupling of the modes around 120 cm^{-1} to the electronic transition is at 4 K a factor of about 1000 weaker.

It is interesting to note that such temperature dependence of the absorption spectrum seems to be characteristic for LHCII (and maybe also the other members of the Chl *a*/*b* xanthophyll binding protein family[32]). The absorption spectra of other Chl *a* binding proteins, the reaction centers of photosystem I[33] and II,[12] and CP47[6] seem to show far less temperature dependence (with respect to width and band positions) than LHCII. The relatively high density of pigments in LHCII (about 30% by mass) and the role that the pigments seem to play in stabilizing the complex[34,35] might be responsible for stronger coupling of the protein dynamics to the pigments at higher temperatures, leading to a temperature dependence of the IDF or electron−phonon coupling.

Vibronic Fine Structure. As shown above we have observed sharp vibronic lines in the emission spectra of LHCII at low temperature. These sharp lines enabled us to identify 48 vibrational modes in the electronic ground state with the corresponding Franck−Condon factors; see Table 1. The vibrational frequencies we observed are compared to those observed with spectral hole burning of Chl *a* in PSI-200 (excited-state vibrations)[29] and fluorescence line narrowing of Chl *a* in ether (both excited and ground-state vibrations).[15] There is a good correspondence between the frequencies of the modes for Chl *a* obtained in different environments and using different techniques. In contrast to the other studies, we observed modes below 250 cm^{-1} and above 1550 cm^{-1}. There is a large difference in the Franck−Condon factors compared to those measured for the first excited state with spectral hole burning.[29] The comparison of the simulated and experimental site-selective fluorescence spectra (Figure 9) shows that the Franck−Condon factors we have estimated are in good agreement with the experiment. A similar simulation of the Chl *a* site spectrum[36] using the Franck−Condon factors of Gillie et al.[29] yields a spectrum with much higher intensities of the vZPLs than those observed here. It should be noted that the estimated Franck−Condon factors all are very low (<0.0015), indicating very weak vibronic coupling in Chl *a*. These small Franck−Condon factors might seem to be in conflict with the absorption spectrum of isolated Chl *a*, which has quite some intensity in the region of 900−1400 cm^{-1}.[25] However, there is clear evidence that the absorption in this region is to a large extent due to the Q_x-transition.[25,37] Fluorescence only takes place from the lowest (Q_y) singlet state. The Q_x transition does not contribute to Chl *a* emission spectra. A comparison between absorption and emission spectra of of Chl *a* clearly shows that the intensity in this region is far more intense in the absorption spectrum than in the emission spectrum.[19,25] A comparison of the vibrational frequencies with the results from resonance Raman studies[38−43] also yields a general agreement. Interesting to note is that the low-frequency (260 cm^{-1} and below) vibrations we observe are the same (within a few wavenumbers) as those recently measured with Q_y-resonance Raman for Chl *a* in solid film.[43] These low-frequency vibrations can show up as oscillations in ultrafast absorption transients.[43,44]

Several of the higher frequency vibrations observed are "markers" of the interactions of the protein environment with the Chl *a* molecule(s) responsible for the emission of LHCII at 4 K.[39,40] The vibronic line observed at 1673 cm^{-1} can be assigned to the C═O stretch mode of the 13^1-keto group.[38] The

frequency suggests that the keto-oxygen is hydrogen bonded to the protein.[39] Also the line at 1645 cm^{-1} might reflect this C═O stretch. The frequency is quite extreme for the C═O stretch of the 13^1-keto group in Chl *a* and has only been observed in Chl *a*−water aggregates,[38,39,42] in which a water molecule at the same time serves as the ligand for the Mg of one Chl molecule and the hydrogen-bond donor for the 13^1-keto group of another. Due to strong excitonic interactions, the Q_y transition is shifted to 740−750 nm in these aggregates. Such a shift is not observed in LHCII, indicating that the large shift of the C═O stretch frequency is caused by another mechanism of very strong hydrogen bonding, possibly by a protonated amino acid. The observation of two C═O stretch frequencies could mean that the emitting state is delocalized over (at least) two different Chl *a* molecules or that we observe emission from (at least) two independent Chl *a* molecules. We cannot distinguish between these two possiblities. In the Chl *a* Soret-excited resonance Raman spectra of trimeric and aggregated LHCII, measured by Ruban and co-workers,[45] a complex set of 13^1-keto C═O stretch frequencies was observed, extending from 1640 to 1710 cm^{-1}. Whereas in the Raman spectra all Chl *a* molecules are observed, here only the subset is detected which is involved in emission upon selective excitation at 4 K, with the C═O stretch frequency at 1645 and 1672 cm^{-1}.

The lines at 1537, 1553, and 1612 cm^{-1} in our spectra (which have been assigned to C═C stretch modes of the chlorin backbone[41]) indicate that the central magnesium has one external ligand.[40,42]

Simulations of the Lowest Energy Absorbing State in LHCII at 4 K. To test more rigorously whether our data can be explained with only one inhomogeneously broadened band around 676 nm[19] or whether a second band in the red wing of the LHCII absorption profile must be invoked, we simulated the selective emission, hole-burning,[21] and T−S[27] spectra of LHCII recorded at 4 K on the basis of the approach of van Mourik and co-workers.[46] We simulated the red-most part of the LHCII absorption spectrum (starting from the 676 nm band) as a cluster of a certain amount of pigments of which the transition frequency was distributed over one or more IDFs. With a cluster we mean a group of pigments which are close enough to efficiently exchange their excitations or, more generally, a collection of states between which rapid energy transfer takes place. No energy transfer is possible between states from different clusters. For these simulations we assume that only downhill energy transfer takes place at 4 K and that emission, intersystem crossing, and hole burning only take place from the zero-phonon level of the lowest energy pigment within a cluster. This last assumption implies fast and complete energy transfer or relaxation to the lowest energy state within a cluster. The total absorption spectrum $A_{tot}(\lambda)$ is built up from contributions of different inhomogeneous distributions

$$A_{tot}(\lambda) = \sum_i A_i(\lambda) = \sum_i n_i[\mathrm{IDF}_i(\lambda) \otimes l(\lambda)] \qquad (7)$$

in which $A_i(\lambda)$ *is* the absorption of distribution *i* at wavelength λ, n_i is the amount of molecules contributing to *i*, $\mathrm{IDF}_i(\lambda)$ is the normalized inhomogeneous distribution function of *i*, $\otimes$ is the convolution operator, and $l(\lambda)$ is the homogeneous line shape: a δ function as ZPL and the PW of Figure 9 (in an area ratio PW/ZPL of 0.822 ($e^{+S} - 1$, with $S = 0.6$, see above)). Here we assumed that the different states have equal dipole strength. The ZPLs correspond to the levels from which fluorescence, energy transfer, intersystem crossing, and hole burning take place. The probability $P_{zpl}(\lambda)$ that a ZPL at excitation wavelength λ is the lowest one within a cluster can be calculated as

$$P_{zpl}(\lambda) = \sum_i \left\{ \frac{n_i \mathrm{IDF}_i(\lambda)}{\sum_k n_k \mathrm{IDF}_k(\lambda)} \right\} \times \{(\int_0^\lambda \mathrm{IDF}_i(\lambda)\, d\lambda)^{n_i - 1} [\prod_{j \neq i} (\int_0^\lambda \mathrm{IDF}_j(\lambda)\, d\lambda)^{n_j}]\} \qquad (8)$$

where *i*, *j*, and *k* run over the inhomogeneous distributions that describe the spectrum. From this probability the spectrum, $A_{low}(\lambda)$, of the lowest energy absorbing state within a cluster (the "trap") can be calculated

$$A_{low}(\lambda) = [\{\sum_k n_k \mathrm{IDF}_k(\lambda)\} P_{zpl}(\lambda)] \otimes l(\lambda) \qquad (9)$$

In principle the trap spectrum should then be the (nonselectively excited) hole-burning spectrum. In a similar way, but now using the line shape of emission, the low-temperature fluorescence spectrum can be calculated. The total probability, $P_{tot}(\lambda)$, of exciting at wavelength λ a lowest energy absorbing state within a cluster can be calculated as

$$P_{tot}(\lambda) = \frac{A_{low}(\lambda)}{A_{tot}(\lambda)} \qquad (10)$$

$P_{tot}(\lambda)$ can be compared directly to the anisotropy of emission if we assume that the anisotropy is zero if energy transfer or relaxation between exciton levels takes place, whereas it is $r_{max} \sim 0.4$ if the excitation remains in the same state. In this crude approximation the expected anisotropy is given by

$$r(\lambda) = P_{tot}(\lambda) r_{max} \qquad (11)$$

We show the results of simulations based on three models for the low-energy side of the Q_y absorption spectrum of LHCII: (1) one Gaussian-shaped IDF (at 676 nm) containing 12 states per cluster, (2) two Gaussian-shaped IDFs (at 675.8 and 680 nm, containing 11 and 1, respectively, states per cluster) (this agrees with the spectral decomposition proposed by Reddy and co-workers[21]), and (3) one non-Gaussian IDF, which is described as the sum of two Gaussians (both at 675.8 nm) with different width containing 12 states per cluster. The number of states per cluster is estimated from the relative oscillator strength of the 676 nm absorption band, which corresponds to 4 Chl's per monomer and 12 per trimer.[19,21] The simulations are not very sensitive on the cluster size, unless values smaller than about nine are taken. The chosen IDFs are not optimal but give reasonable descriptions. The results of the simulations are shown in Figure 10.

A comparison between the red-most part of the measured and constructed absorption spectra (Figure 10A) reveals that (at least) two Gaussians (convoluted with the PW) are needed for a reasonable description (models 2 and 3); a single one cannot describe the red edge of the band well (1). Very similar results could be obtained using many other combinations of two Gaussians (not shown). All these descriptions yielded very similar results in the simulations given below.

For all three simulations the absorption spectra calculated for the trap (Figure 10B) peak near 679.5 nm (679.4 for simulation 1, 679.7 for 2, and 679.5 for 3). This agrees well with the 4 K T−S spectrum[23] and the hole-burning[21] spectrum, peaking at 680 nm. The widths, however, of the simulated spectra are narrower than those of the experimental spectra (5.5−6 nm[21,23]). For simulations 2 (4.4 nm fwhm) and 3 (4.2 nm), the difference

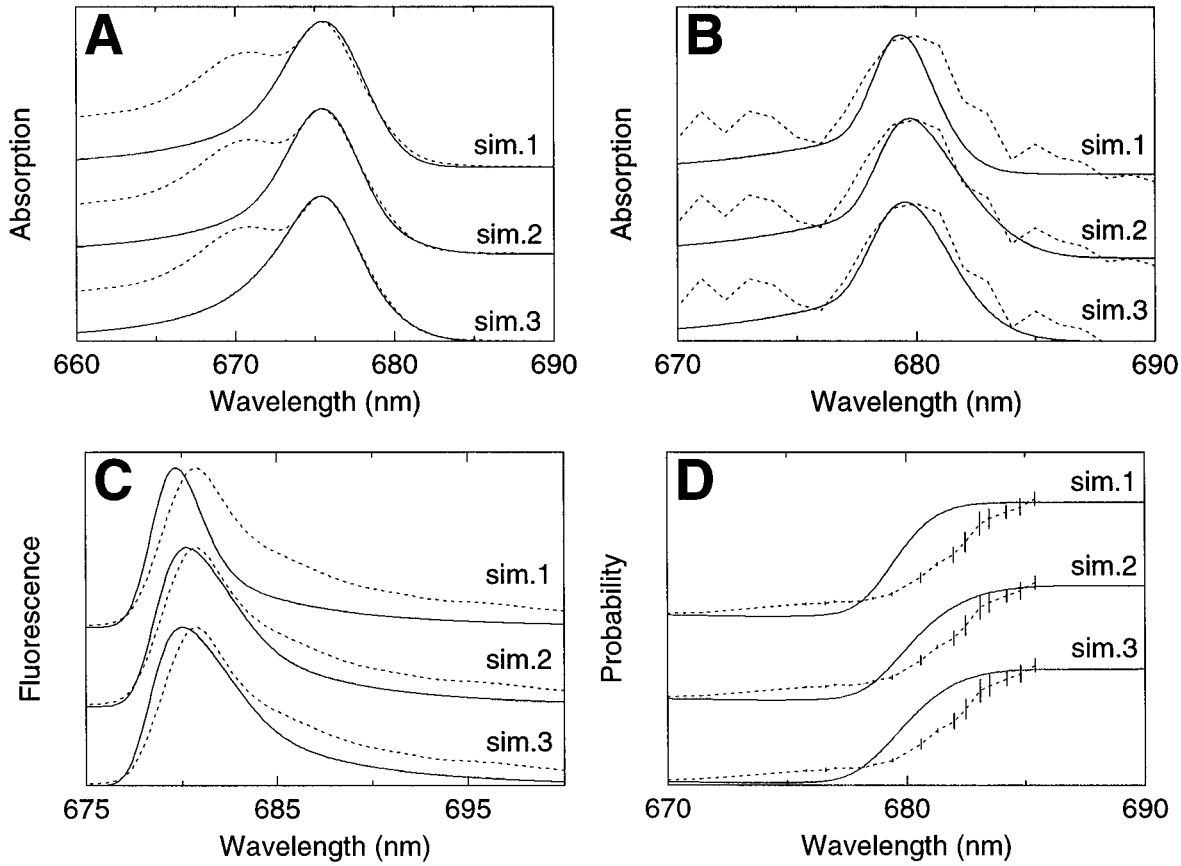

Figure 10. Results of the simulations of the lowest energy absorbing state in LHCII (see text), describing the red part of the absorption spectrum using one Gaussian IDF at 676 nm (sim. 1); two Gaussian IDFs at 675.8 and 680 nm (sim. 2); one IDF which is the sum of two Gaussians, both at 675.8 nm (sim. 3). Comparison between (A) experimental 4 K absorption spectrum (dashed lines) and the spectra used for the simulations (solid lines); (B) the experimental 4 K Chl *a* T−S spectrum[27] (dashed lines) and the simulated trap absorption spectra (solid lines); (C) the experimental (nonselective) 4 K emission spectrum (dashed lines) and the simulated trap emission spectra (solid lines); (D) the experimental 4 K emission anisotropy curve (dashed lines) and the simulated probability of directly exciting a trap (scaled to the maximum anisotropy, solid lines). For a good comparison the spectra of the different simulations were given equidistant offsets.

is about 1 nm, but for 1 (3.3 nm) the difference is significantly larger. Interesting to note is that for simulation 2 about 63% of the trap is in fact part of the 676 inhomogeneous distribution and only 37% of the 680 nm one, indicating that if a 680 nm state is present, it does not dominate the trap spectrum. It should be noted that the agreement between the experimental and simulated widths can be improved by reducing the effective cluster size ($N < 9$). A decrease of the effective cluster size might occur if not all excitations are able to reach the lowest energy state or if strong excitonic interactions might cause a smaller number of excitonic transitions to dominate the long-wavelength part of the spectrum. However this would also lead to a blue shift of the trap spectrum for $N < 9$, in disagreement with the experimental results. Therefore the position of the maximum indicates that a large number of states with more or less similar dipole strength ($N > 9$) contribute to the absorption band around 676 nm. On the other hand, a small fraction of isolated pigments absorbing near 677 nm might lead to a slight broadening of the trap spectrum, which could explain the difference between simulated and observed widths.

In Figure 10C a comparison is shown of the experimental emission spectrum (at 4 K, upon aselective excitation) and the simulated emission spectra. For all models the simulated emission maximum (679.7 nm for 1, 680.3 for 2, and 680.0 nm for 3) is somewhat to the blue of the experimental value (680.7 nm), like the trap absorption spectra. The width of the emission from the trap is always larger than that of the trap absorption spectrum, especially for simulations 2 and 3. This is due to the asymmetric shape of the distribution of ZPLs of the traps. The widths of 2 (5.3 nm) and 3 (5.5 nm) agree very well to the experimental width (5.7 nm); the width of 1 is far off (3.6 nm). Although peak position and width can be simulated rather well, the simulations underestimate the red wing (>685 nm) of the emission spectra.

The simulations (Figure 10D) all yield a steep increase of $P_{tot}(\lambda)$ from zero to maximum in a few nanometers around 680 nm. This is qualitatively in agreement with the anisotropy (Figure 6) measured at 4 K, which rises above 679 nm steeply to a value of 0.36 at 685 nm and the steep ingrowth of the intensity of the vibronic lines above ~679 nm, which reach constant intensity above 680.5 nm. However, the steep part of the ingrowth of the anisotropy seems to be shifted about 1 nm to the red, compared to simulations 2 and 3 of $P_{tot}(\lambda)$; for simulation 1 the shift is even bigger. This quantitative difference between experiment and simulation is in line with the difference in position and width of the simulated trap spectrum and the experimental T−S and hole-burning spectra (Figure 10B). A possible explanation for these discrepancies is that the states at the red-most edge have slightly less dipole strength than the ones that are located more to the blue (possibly due to excitonic interactions).

In conclusion, the simulations of the trap spectrum show that the absorption spectrum of LHCII above 676 nm cannot be described with a single Gaussian IDF. Simulations with a non-Gaussian IDF or two IDFs are considerably better. Although we cannot favor one or the other explanation, we conclude that a large number of states (>9) per trimer contribute to the absorption band at 676 nm and that the dipole strengths of these

states should be of the same order of magnitude as that of monomeric Chl *a*. This can be easiest understood in terms of monomeric Chl *a* molecules but also holds if excitonic coupling does not lead to states with a dipole strength which deviates considerably from that of monomeric Chl *a*.

Conclusions

We have observed single-site spectra in the emission of LHCII at 4 K. In these spectra apart from the zero-phonon line a separate phonon wing and 48 vibronic lines are observed. The vibronic frequencies indicate that the emitting Chl *a* is monoligated and accepts a hydrogen bond. Using the phonon wing from the 4 K emission spectra, we have simulated the temperature dependence of the width of the absorption spectrum. We can explain this temperature dependence up to 220 K by weak ($S = 0.6 \pm 0.1$) linear, harmonic Franck−Condon electron−phonon coupling and a temperature independent inhomogeneous width (120 ± 15 cm^{-1}). Simulations of the spectroscopic properties of the lowest energy states at 4 K show that the lowest energy absorption band (peaking near 676 nm) consists of at least nine separate electronic states (per LHCII trimer). The band is inhomogenously broadened but cannot be described using one, Gaussian inhomogeneous distribution function. The simulations cannot distinguish between a model with two Gaussian inhomogeneous distributions (at 676 and 680 nm with intensity 11 and 1) or with a single, non-Gaussian distribution (at 676 nm).

Acknowledgment. This work was supported by the Netherlands Foundation for Scientific Research (NWO) via the Foundation for Life Sciences (SLW) and the European Union (contract number 94 0619). We thank Florentine Calkoen for preparation of the LHCII, Dr. B. Robert for stimulating discussions, and the reviewers for useful comments.

References and Notes

(1) Van Grondelle, R.; Dekker, J. P.; Gillbro, T.; Sundström, V. *Biochim. Biophys. Acta* **1994**, *1187*, 1.
(2) Rebane, K. K. *Impurity spectra of solids*; Plenum Press: New York, 1970.
(3) Personov, R. I. In *Spectroscopy and excitation dynamics of condensed molecular systems*; Agranovich, V. M., Hochstrasser, R. M., Eds.; North Holland: Amsterdam, 1983; Chapter 10.
(4) Renge, I.; Avarmaa, R. *Photochem. Photobiol.* **1985**, *42*, 253.
(5) Eccles, J.; Honig, B. *Proc. Natl. Acad. Sci. U.S.A.* **1983**, *80*, 4959.
(6) Renge, I; Dekker, J. P.; van Grondelle, R. *J. Photochem. Photobiol. A* **1996**, *96*, 109.
(7) Friedrich, J.; Haarer, D. *Angew. Chem.* **1984**, *96*, 96.
(8) Jankowiak, R.; Hayes, J. M.; Small, G. J. *Chem. Rev.* **1993**, *93*, 1471.
(9) Cupane, A.; Leone, M.; Vitrano, E.; Cordone, L. *Eur. Biophys. J.* **1995,** *23*, 385.
(10) Hayes, J. M.; Lyle, P. A.; Small, G. J. *J. Phys. Chem.* **1994**, *98*, 7337.
(11) Pullerits, T.; Monshouwer, R.; van Mourik, F.; van Grondelle, R. *Chem. Phys.* **1995**, *194*, 395.
(12) Konermann, L.; Holzwarth, A. R. *Biochemistry* **1996**, *35*, 829.
(13) Zucchelli, G.; Garlaschi, F. M.; Finzi, L.; Jennings, R. C. In *Photosynthesis: from Light to Biosphere*; Mathis, P., Ed.; Kluwer Academic Publishers: Dordrecht, The Netherlands, 1995; Vol. I, p 179.
(14) Lutz, M; Mäntele, W. In *The Chlorophylls*; Scheer, H., Ed.; CRC Press: Boca Raton, FL, 1991; Chapter 4.6.
(15) Avarmaa, A. A.; Rebane, K. K. *Spectrochim. Acta* **1985**, *41A*, 1365.
(16) Bykovskaya, L. A.; Litvin, F. F.; Personov, R. I.; Romanovskii, Yu. V. *Biophysics* **1980**, *25*, 8.
(17) Jansson, S. *Biochim. Biophys. Acta* **1994**, *1184*, 1.
(18) Kühlbrandt, W.; Wang, D. N.; Fujiyoshi, Y. *Nature* **1994**, *367*, 614.
(19) Hemelrijk, P. W.; Kwa. S. L. S.; van Grondelle, R.; Dekker, J. P. *Biochim. Biophys. Acta* **1992**, *1098*, 159.
(20) Nussberger, S.; Dekker, J. P.; Kühlbrandt, W., van Bolhuis, B. M.; van Grondelle, R.; van Amerongen, H. *Biochemistry* **1994**, *33*, 14775.
(21) Reddy, N. R. S.; van Amerongen, H.; Kwa, S. L. S.; van Grondelle, R.; Small, G. J. *J. Phys. Chem.* **1994**, *98*, 4729.
(22) Savikhin, S.; van Amerongen, H.; Kwa, S. L. S.; van Grondelle, R.; Struve, W. S. *J. Phys. Chem.* **1994**, *98*, 1597.
(23) Peterman, E. J. G.; Dekker, J. P.; van Grondelle, R.; van Amerongen, H.; Nussberger, S. *Lithuanian J. Phys.* **1994**, *34*, 301.
(24) Kwa, S. L. S.; Groeneveld, F. G.; Dekker, J. P.; van Grondelle, R.; van Amerongen, H.; Lin, S.; Struve, W. *Biochim. Biophys. Acta* **1992**, *1101*, 143.
(25) Kwa, S. L. S.; Völker, S.; Tilly, N. T.; van Grondelle, R.; Dekker, J. P. *Photochem. Photobiol.* **1994**, *59*, 219.
(26) Krawczyck, S; Krupa, Z.; Maksymeic,W. *Biochim. Biophys. Acta* **1993**, *1143*, 273.
(27) Peterman, E. J. G.; Dukker, F. M.; van Grondelle, R.; van Amerongen, H. *Biophys. J.* **1995**, *69*, 2670.
(28) Lokstein, H.; Leupold, D.; Voigt, B.; Nowak, F, Ehlert, J.; Hoffmann, P.; Garab, G.; *Biophys. J.* **1995**, *69*, 1536.
(29) Gillie, J. K.; Small, G. J.; Goldbeck, J. H. *J. Phys. Chem.* **1989**, *93*, 1620.
(30) Van Amerongen, H.; Kwa, S. L. S.; van Bolhuis, B. M.; van Grondelle, R. *Biophys. J.* **1994**, *67*, 837.
(31) Visser, H. M.; Somsen, O. J. G.; Van Mourik, F.; Van Grondelle, R. *J. Phys. Chem.* **1996**, *100*, 18859.
(32) Zucchelli, G.; Dainese, P.; Jennings, R. C.; Breton, J.; Garlaschi, F. M.; Bassi, R. *Biochemistry* **1994**, *33*, 8982.
(33) Pålsson, L. O.; Dekker, J. P.; Schlodder, E.; Monshouwer, R.; van Grondelle, R. *Photosynth. Res.* **1996**, *48*, 239.
(34) Plumley, F. G.; Schmidt, G. W. *Proc. Natl. Acad. Sci. U.S.A.* **1987**, *84*, 146.
(35) Paulsen, H.; Finkenzeller, B.; Kühlein, N. *Eur. J. Biochem.* **1993**, *215*, 809.
(36) Struve, W. S. In *Anoxygenic Photosynthetic Bacteria*; Blankenship, R. E., Madigan, M. T., Bauer, C. E., Eds.; Kluwer Academic Publishers: Dordrecht, The Netherlands, 1995; Chapter 15.
(37) Krawczyck, S. *Biochem. Biophsy. Acta* **1991**, *1056*, 64.
(38) Lutz, M. *J. Raman Spectrosc.* **1974**, *2*, 497.
(39) Koyama, Y.; Umemoto, Y.; Akamatsu, A.; Uehara, K.; Tanaka, M. *J. Mol. Struct.* **1986**, *146*, 273.
(40) Fujiwara, M.; Tasumi, M. *J. Phys. Chem.* **1986**, *90*, 250.
(41) Fujiwara, M.; Tasumi, M. *J. Phys. Chem.* **1986**, *90*, 5646.
(42) Sato, H.; Okada, K; Uehara, K.; Ozaki, Y. *Photochem. Photobiol.* **1995**, *61*, 175.
(43) Diers, J. R.; Zhu, Y.; Blankenship, R. E.; Bocian, D. F. *J. Phys. Chem.* **1996**, *100*, 8573.
(44) Chachisvilis, M.; Fidder, H.; Pullerits, T.; Sundström, V. *J. Raman Spectrosc.* **1995**, *26*, 513.
(45) Ruban, A. V.; Horton, P.; Robert, B. *Biochemistry* **1995**, *34*, 2333.
(46) Van Mourik, F.; Visschers, R. W.; van Grondelle, R. *Chem. Phys. Lett.* **1992**, *195*, 1